



Zika but not Dengue virus infection limits NF- κ B activity in human monocyte-derived dendritic cells and suppresses their ability to activate T cells

Received: 17 August 2024

Accepted: 4 March 2025

Published online: 25 March 2025

 Check for updates

Ying-Ting Wang¹, Emilie Branche¹, Jialei Xie², Rachel E. McMillan^{2,3},
Fernanda Ana-Sosa-Batiz¹, Hsueh-Han Lu^{1,3}, Qin Hui Li^{1,3}, Alex E. Clark^{1,2},
Joan M. Valls Cuevas¹, Karla M. Viramontes¹, Aaron F. Garretson^{1,2},
Rúbens Prince dos Santos Alves¹, Sven Heinz^{1,2}, Christopher Benner²,
Aaron F. Carlin^{2,4}  & Sujan Shresta^{1,5} 

Understanding flavivirus immunity is critical for the development of pan-flavivirus vaccines. Dendritic cells (DC) coordinate antiviral innate and adaptive immune responses, and they can be targeted by flaviviruses as a mechanism of immune evasion. Using an unbiased genome-wide approach designed to specifically identify flavivirus-modulated pathways, we found that, while dengue virus (DENV) robustly activates DCs, Zika virus (ZIKV) causes minimal activation of genes involved in DC activation, maturation, and antigen presentation, reducing cytokine secretion and the stimulation of allogeneic and peptide-specific T cell responses. Mechanistically, ZIKV inhibits DC maturation by suppressing NF- κ B p65 recruitment and the subsequent transcription of proinflammatory and DC maturation-related genes. Thus, we identify a divergence in the effects of ZIKV and DENV on the host T cell response, highlighting the need to factor such differences into the design of anti-flavivirus vaccines.

Zika virus (ZIKV) and dengue virus (DENV) are positive-sense single-stranded RNA viruses of the genus *Flavivirus*, which includes other clinically important pathogens such as yellow fever virus, West Nile virus, and Japanese encephalitis virus. ZIKV and DENV share considerable antigenic homology, have similar modes of transmission, and co-circulate in many regions of the world¹. Most infections with either ZIKV or DENV lead to mild, self-limiting illnesses consisting mainly of fever, rash, and headache². However, both viruses can cause severe and sometimes life-threatening diseases, albeit with markedly different clinical manifestations. For example, ZIKV infection in pregnant

women may affect fetal brain development and lead to congenital Zika syndrome, and infection in children and adults has been linked to neurological symptoms and Guillain-Barré syndrome, respectively². In contrast, severe DENV infection is characterized by fever, hemorrhage, shock, and even death².

Dendritic cells (DC) function in both the innate and adaptive immune responses through their ability to recognize invading pathogens and present antigens to T cells³. Upon recognition of microbial molecules through intracellular and cell surface pathogen recognition receptors, DCs undergo a maturation program accompanied by

¹Center for Vaccine Innovation, La Jolla Institute for Immunology, La Jolla, CA, USA. ²Department of Medicine, School of Medicine, University of California, San Diego, La Jolla, CA, USA. ³Biomedical Sciences Graduate Program, University of California, La Jolla, California, USA. ⁴Department of Pathology, School of Medicine, University of California, San Diego, La Jolla, CA, USA. ⁵Department of Pediatrics, Division of Host-Microbe Systems and Therapeutics, University of California, San Diego, La Jolla, CA, USA. ✉ e-mail: acarlin@health.ucsd.edu; sujan@lji.org

upregulation of major histocompatibility complex (MHC) and costimulatory molecules, secretion of cytokines, and migration to local secondary lymphoid organs, where they present antigen to activate naïve T cells⁴. Thus, DCs shape the antigen-specific adaptive immune response by supplying the three key signals, namely antigen/MHC, costimulatory molecules, and cytokines, all of which are necessary for the activation and/or differentiation of naïve and primed T cells.

DCs also initiate antiviral responses and are major cellular hosts for flaviviruses. Both ZIKV and DENV replicate extensively in DCs; however, the effects of ZIKV and DENV infection on the activation, maturation, and function of human DCs remain poorly understood, and several studies have yielded conflicting reports^{5–11}. Previous findings have demonstrated that ZIKV-infected individuals elicit modest immune response¹² and short-lived anti-ZIKV neutralizing antibody levels¹³. Moreover, suppressed antigen-presenting capacity of DCs resulting in delayed ZIKV clearance was also reported in ex vivo⁷ and in vivo models¹⁴.

In the current study, we employ a method to discretely analyze virus-infected and uninfected bystander cells to identify how ZIKV and DENV alter human DC function at the genomic, molecular, and cellular levels. Despite their genetic similarities, we find that ZIKV and DENV elicit distinct transcriptional responses in infected human monocyte-derived DCs (moDCs). Whereas DENV stimulates NF- κ B p65 recruitment to and transcription of inflammatory genes, leading to proinflammatory cytokine production and T cell activation, ZIKV infection suppresses NF- κ B p65-associated gene transcription and consequently impairs DC activation, maturation, and the ability to stimulate allogeneic and peptide-specific T cell responses. These findings identify a key mechanism of immune evasion by ZIKV and highlight the distinct effects of closely related flaviviruses on the host immune system.

Results

ZIKV and DENV Stimulate distinct transcriptional programs in infected human monocyte-derived DCs

Genome-wide transcriptional analysis can identify mechanisms by which viruses alter host responses in an unbiased and comprehensive manner. However, bulk analysis of mixed infected and uninfected cell populations can obscure virus-specific effects^{15–17}. Therefore, to identify transcriptional changes specifically in ZIKV- or DENV-infected DCs, we utilized our previously described virus-specific genomics approach to separate virus-infected human blood monocyte-derived DCs (moDC) (referred to as virus+, ZIKV+, or DENV+) from uninfected bystander moDCs (virus–, ZIKV–, or DENV–) from the same cultures and then performed RNA-seq on the separated cell populations¹⁵. Immature moDCs were infected with ZIKV SD001, an Asian lineage strain isolated in 2016, or DENV2 UIS353 (serotype 2), which was isolated from a Colombian patient in 2016, at multiplicities of infection (MOI) of 0.5 and 1, respectively, for 24 h. We showed previously that the two viruses infect moDCs with similar kinetics, peaking at 24 h post-infection (hpi)¹⁷. Virus+ and virus– moDCs were purified by staining for ZIKV or DENV envelope (E) protein using the pan-flaviviral E protein antibody 4G2 followed by fluorescence-activated cell sorting (Fig. 1a). This method effectively separated virus+ and virus– cells, as determined by analysis of RNA-seq reads aligning to the viral genome (Supplementary Fig. 1a). Principal component analysis (PCA) of gene expression profiles in moDCs derived from three healthy donors demonstrated that both the infection status and virus species significantly affected the cellular transcriptional response, whereas inter-donor differences were less influential (Fig. 1b). Consistent with the PCA results, many genes were regulated based on infection status, (e.g., tumor necrosis factor [TNF] receptor superfamily member 10b [*TNFRSF10B*]) and/or in a virus-specific manner (e.g., stearoyl-CoA desaturase [*SCD*] and tribbles homolog 3 [*TRIB3*]) (Fig. 1c). Virus-specific transcriptional effects would be expected to occur selectively in virus+ cells, whereas environmental signals would be expected to

elicit a response in both virus+ and bystander cells (Supplementary Fig. 1b). Thus, by comparing the transcriptional responses of virus+ or virus– cells with that of mock-infected (mock) moDCs, we were able to identify subsets of genes that were either induced by or suppressed by virus infection (Supplementary Fig. 1c). For example, interferon (IFN)-beta (*IFNB*) was selectively upregulated in virus+ moDCs compared with the corresponding bystander cells, likely due to intracellular pattern receptor recognition of virus products found only in infected cells (Supplementary Fig. 1b). In contrast, virus+ moDCs exhibited reduced expression of IFN-stimulated genes (ISGs), including *MX1* and *MX2*, compared with bystander moDCs (Supplementary Fig. 1d), which is consistent with the known ability of these viruses to inhibit the ISG factor 3 (ISGF3) signaling complex (Supplementary Fig. 1b and d)¹⁸.

Virus-regulated genes were identified as those significantly upregulated or downregulated in virus+ cells compared with both virus– bystander and mock moDCs derived from three matched donors (Supplementary Fig. 1e and f). Surprisingly, the virus-regulated gene sets in ZIKV+ and DENV+ moDCs were largely nonoverlapping; that is, of the 131 and 478 genes specifically upregulated in ZIKV+ and DENV+ cells, respectively, only 33 were shared (Fig. 1d). Similarly, only 16 genes were commonly downregulated in ZIKV+ and DENV+ moDCs (Fig. 1e). Functional enrichment analysis demonstrated that genes exclusively upregulated by DENV were associated with cytokine and inflammatory signaling and migration (Fig. 1f, yellow box), whereas genes exclusively upregulated by ZIKV were involved in lipid metabolism pathways (Fig. 1f, red box)¹⁷. The functions of virus-downregulated genes also differed between ZIKV+ and DENV+ moDCs. Specifically, infection with ZIKV, but not DENV, resulted in the downregulation of genes involved in multiple essential DC functions, such as antigen processing and presentation, differentiation, and migration (Fig. 1g, blue box).

We next analyzed bystander virus– cells to determine how infected cells might communicate through secretion of signaling molecules (Supplementary Fig. 1b). Comparing differential gene expression between ZIKV– and DENV– moDCs, we found that 559 genes functionally involved in cellular activation and TNF signaling (e.g., *TNF*, *LTA*, and *TNFAIP3*) were upregulated to a significantly greater extent in DENV– moDCs than in ZIKV– moDCs; and conversely, 146 viral response and ISGs (e.g., interferon-induced transmembrane [*IFITM*] proteins 1–3 and cholesterol 25-hydroxylase [*CH25H*]) were upregulated to a significantly greater extent in ZIKV– moDCs than in DENV– moDCs (Supplementary Fig. 1g and h).

Collectively, these results demonstrate that DENV and ZIKV infection of moDCs induce markedly different transcriptional programs that also influence uninfected bystander cells, most likely via secretion of IFNs and other cytokines. In addition, ZIKV+ moDCs express lower levels of many inflammatory genes than do DENV+ moDCs.

ZIKV Infection Limits the Ability of Human Monocyte-Derived DCs to Mature and Produce Cytokines

Infection of or antigen uptake by immature DCs activates a transcriptional maturation program that modifies cell surface and secretory phenotypes to allow DC migration and to attract and activate antigen-specific T cells. Our RNA-seq pathway analysis suggested that ZIKV+ moDCs have reduced transcriptional responses that may limit key DC functions. To examine the effect of ZIKV *vs* DENV infection on the DC maturation-associated phenotype and function in more detail, we first compared the expression of 19 costimulatory molecules and 16 cytokines involved in DC migration and T cell activation. We found that DENV+ moDCs expressed 14 costimulatory molecules and 12 cytokines at significantly higher levels than did ZIKV+ moDCs (Fig. 2a). We also evaluated cell surface expression of costimulatory molecules and secretion of proinflammatory cytokines in virus+ *vs* mock moDCs. As a positive control, moDCs were treated with lipopolysaccharide (LPS),

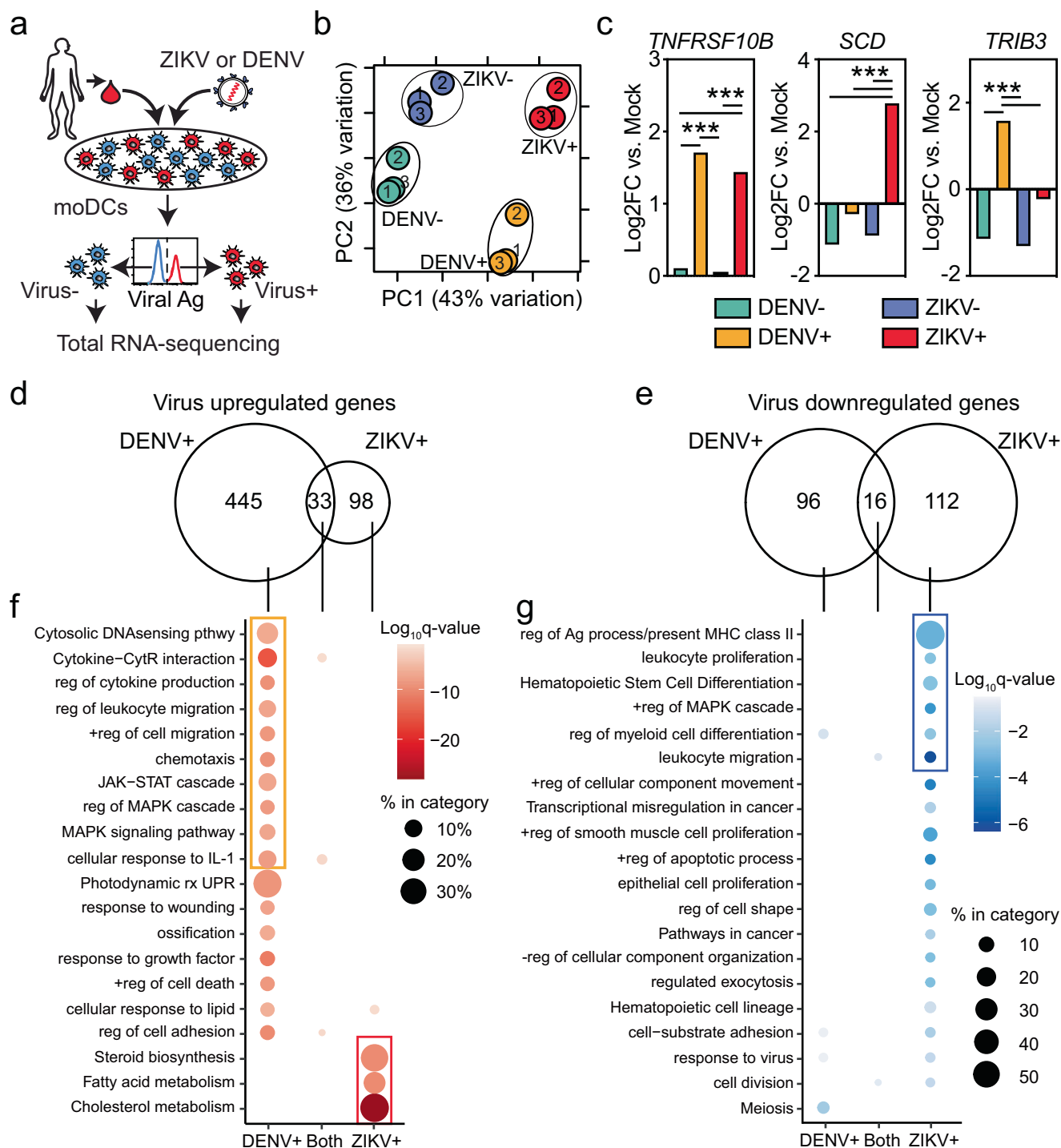
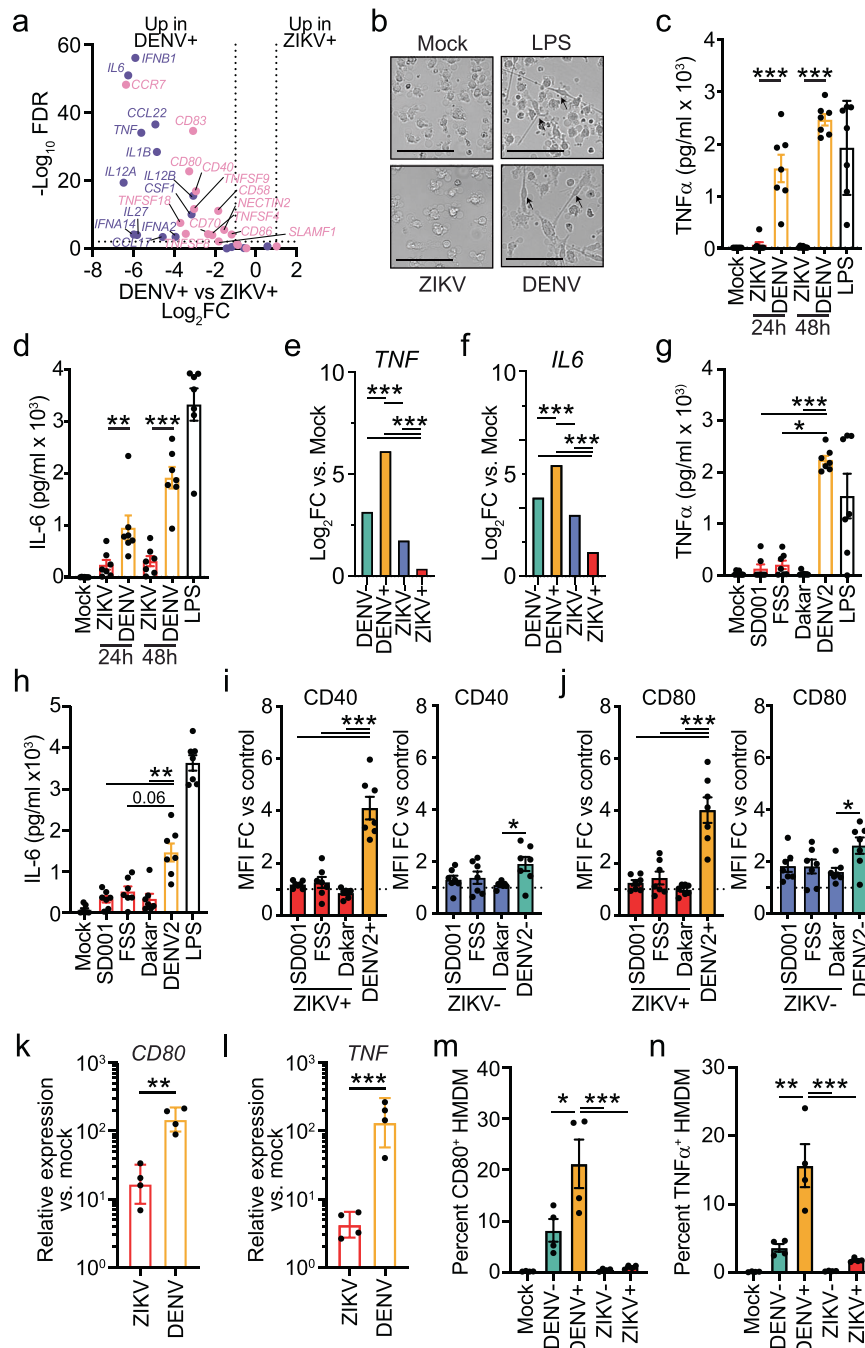


Fig. 1 | ZIKV and DENV Infection Induce Distinct Transcriptional Programs in Human moDCs. **a** Experimental strategy. Freshly isolated monocytes from three healthy donors were differentiated into moDCs by incubation with GM-CSF and IL-4 for 7 days and then infected with ZIKV SD001 or DENV2 UIS353 (MOI 0.5 and 1, respectively) for 24 h, sorted into virus-infected (ZIKV+/DENV+) and bystander uninfected (ZIKV-/DENV-) populations using the pan-flaviviral E antibody 4G2, and subjected to RNA-seq. Mock-infected cells were processed in an identical manner. **b** Principal component analysis (PCA) biplot of gene expression patterns in ZIKV+, ZIKV-, DENV+, and DENV- moDCs compared with mock-infected cells. Circles labeled 1–3 represent individual donors. **c** mRNA expression (RNA-seq) of *TNFRSF10B*, *SCD*, and *TRIB3* in purified virus + and virus - moDCs at 24 h post-

infection (hpi). Data are expressed as the log2 fold change (FC) relative to mock-infected cells with a two-sided false discovery rate calculated by DESeq2 corrected for multiple hypothesis testing using the Benjamin-Hochberg correction.

*** $P < 0.001$. **d, e** Venn diagrams showing the number of unique and shared genes (d) upregulated or (e) downregulated in virus + moDCs at 24 hpi. **f, g** Metascape analysis of unique and shared genes (f) upregulated or (g) downregulated in virus + moDCs at 24 hpi. Red and blue intensity represents the magnitude of differential expression, circle size represents the percentage of genes within each category. Yellow, red, and blue boxes contain genes associated with cytokine and inflammatory signaling, lipid metabolism, and essential DC functions, respectively.



which induces DC maturation by binding to Toll-like receptor 4 (TLR4) and activating the transcription factor (TF) nuclear factor- κ B (NF- κ B)¹⁹. Mock moDCs showed the typical rounded morphology (Fig. 2b) and low cell surface expression of CD40, CD80, CD83, and CD86 expression that are characteristic of immature DCs (Supplementary Fig. 2a and 2b). In contrast, stimulation of moDCs with LPS (24 h) induced an adherent spindle-shaped morphology (Fig. 2b) and upregulated CD40, CD80, CD83, and CD86 expression (Supplementary Fig. 2b), both of which are typical of mature DCs. Notably, ZIKV + moDCs exhibited severely limited maturation compared with DENV + moDCs in terms of both morphology (Fig. 2b) and surface phenotype (Supplementary Fig. 2b). Moreover, secretion of the proinflammatory cytokines IL-6 and TNF was virtually abolished in ZIKV + moDCs compared with DENV + cells at both 24 and 48 hpi (Fig. 2c and d), which is consistent with the RNA-seq results showing that ZIKV + moDCs expressed markedly lower levels of *IL6* and *TNF*, DC migration-

associated genes (*CCR7*, *CCL17*, *CCL22*), and costimulatory receptors (*CD40*, *CD80*, *CD83*, *CD86*) compared with both DENV + and bystander moDCs (Fig. 2e, f and Supplementary Fig. 2c, d). These results demonstrate that the transcriptional maturation program of moDCs is strikingly impaired following ZIKV infection compared with DENV infection, which suggests that ZIKV infection may actively suppress this program.

We next asked whether the observed impairment of cytokine production and maturation in ZIKV + moDCs was restricted to the mid-epidemic Asian lineage ZIKV SD001 or was also observed with other ZIKV strains. moDCs were treated with LPS (control) or infected with ZIKV SD001, ZIKV African strain Dakar-1984, ZIKV Asian pre-epidemic strain FSS13025 (all at MOI of 0.5), or DENV strain UIS353 (as used above; MOI of 1). At 48 hpi, moDCs infected with these diverse ZIKV strains secreted significantly lower levels of IL-6 and TNF (Fig. 2g and h) and expressed significantly lower cell surface levels of CD40, CD80,

Fig. 2 | ZIKV Infection Limits the Activation and Maturation of Human Monocyte-Derived DCs and Macrophages. **a** Volcano plot showing the relative expression of genes encoding cytokines and costimulatory molecules involved in DC migration and activation of T cells in ZIKV + and DENV + moDCs. Data are expressed as the \log_{10} fold change (FC) relative to the two-sided FDR calculated by DESeq2 corrected for multiple hypothesis testing using the Benjamin-Hochberg correction. **b** Morphology of day 7 moDCs at 24 h after mock, ZIKV SD001, or DENV2 infection or treatment with 1 μ g/ml LPS (cells derived from the same donor). Black arrows indicate spindle-shaped mature moDCs. Scale bar, 100 μ m. **c, d** ELISA quantification of **(c)** TNF ($n = 7$ donors) and **(d)** IL-6 ($n = 7$ donors) in supernatants from virus + moDCs at 24 and 48 h post-infection (hpi) and from 1 μ g/ml LPS-stimulated moDCs after 24 h incubation. **e, f** Relative mRNA expression (RNA-seq) of *TNF* and *IL6* in virus + and virus - moDCs at 24 hpi. Data are expressed as the \log_2 FC relative to mock-infected cells with two-sided FDR calculated by DESeq2 corrected for multiple hypothesis testing using the Benjamin-Hochberg correction. *** $P < 0.001$ ($n = 3$ donors). **g, h** ELISA quantification of **(g)** TNF ($n = 7$ donors) and **(h)** IL-6 ($n = 7$ donors) in 24 h supernatants from moDCs infected with ZIKV SD001, ZIKV FSS13025 (FSS), ZIKV Dakar-1984 (Dakar) (all at an MOI of 0.5), or DENV2 UIS353 at an MOI of 1. **i, j** Relative fold change (FC) in mean fluorescence intensity (MFI) of CD40 ($n = 7$ donors) and CD80 ($n = 7$ donors) surface expression in moDCs

infected as in **(g and h)** but for 48 h. Cells were surface stained with antibodies against CD40 and CD80, and intracellularly stained with 4G2 anti-flaviviral E antibody. FC in MFI is relative to mock-infected moDCs derived from the same donor. **k, l** Relative expression of **(k)** *CD80* ($n = 4$ donors) and **(l)** *TNF* mRNA ($n = 4$ donors) (qRT-PCR) in human monocyte-derived macrophages (HMDMs) infected via antibody-dependent enhancement with 4G2 antibody plus ZIKV SD001 or DENV2 UIS353 at a MOI of 1 for 24 h. **m, n** Percentage of mock- and virus-infected HMDMs expressing surface CD80 ($n = 4$ donors) or intracellular TNF ($n = 4$ donors) after incubation for 24 h as described for **(k and l)**. Data are presented as the mean \pm SEM (**c, d, m, n**, and **g–j**) or geometric mean \pm geometric SD (**k and l**). Circles represent the average of at least duplicates from each donor. In **(c and d)**, ZIKV and DENV were compared at each time point using two-sided Mann–Whitney U tests; in **(g and h)**, DENV was compared to each ZIKV strain using the Kruskal–Wallis test with Dunn's correction for multiple comparisons; in **(i and j)**, DENV was compared to each ZIKV strain using repeated measures one-way ANOVA with Dunnett's correction for multiple comparisons; in **(k and l)**, log-transformed DENV and ZIKV relative gene expression was compared using a two-tailed paired *t* test. In **(m and n)**, all groups were compared using repeated measures of one-way ANOVA with Tukey's correction for multiple comparisons. * $P < 0.05$, ** $P < 0.01$, *** $P < 0.001$. Source data and exact *P*-values are provided as a Source Data file.

and CD83 (Fig. 2i and j and Supplementary Fig. 2e) compared with DENV2 + moDCs. Of note, neither the proportion of infected moDCs nor the intracellular viral antigen levels differed between ZIKV + and DENV + cells (Supplementary Fig. 2f and g), indicating that the reduced ability of ZIKV + moDCs to undergo maturation is cell-intrinsic and not due to differences in infection rates or viral antigen loads at the different MOIs. Taken together, these results demonstrate that suppression of moDC maturation is a common attribute of ZIKV strains and is driven, at least in part, by impaired induction of the DC maturation gene expression program.

ZIKV Infection limits maturation and cytokine production by human monocyte-derived macrophages

Because flaviviruses can also infect non-DC antigen-presenting cells, such as macrophages, we performed a similar investigation to determine whether macrophage activation is also limited by infection with ZIKV compared with DENV. Primary macrophages are relatively resistant to flavivirus infection in the absence of antibody-dependent enhancement (ADE) of infection¹⁵; therefore, we infected primary human blood monocyte-derived macrophages (HMDM) by incubation with either ZIKV or DENV (both at MOI of 1) in the presence of the pan-flavivirus E antibody 4G2. At 24 hpi, similar proportions of HMDMs were infected with ZIKV compared with DENV (Supplementary Fig. 3a). Despite this, the relative expression of *CD80*, *TNF*, *IL1B*, and *IL6* was significantly lower in ZIKV + compared with DENV + HMDMs at both the mRNA and protein levels ($P < 0.01$; Figs 2k–n and Supplementary Fig. 3b–d). These findings, therefore, demonstrate that ZIKV infection profoundly limits the maturation and inflammatory gene expression programs of both moDCs and HMDMs.

ZIKV Inhibits moDC maturation and function by suppressing NF- κ B p65 activation

To investigate the transcriptional mechanism by which selective infection with ZIKV impairs DC maturation, we compared the functions of genes differentially expressed in ZIKV + and DENV + moDCs. We identified 1031 genes that were upregulated to a greater degree in DENV + cells compared with ZIKV + moDCs (Fig. 3a). These genes were associated with cytokine and inflammatory signaling, and their promoters were most strongly enriched for motifs recognized by NF- κ B and, to a lesser extent, IFN-stimulated regulatory element/IFN-induced regulatory factor (ISRE/IRF) TFs (Fig. 3b and c). Consistent with our previous analysis¹⁷, ZIKV + moDCs exhibited upregulation of only 56 genes compared with DENV + cells, and these genes were functionally associated with lipid metabolism and regulation (Figs. 1f, 3a, and b). Given the pivotal role of NF- κ B in the induction of DC maturation,

these data suggest that ZIKV may impair moDC maturation and function by failing to optimally activate NF- κ B.

To test this possibility, we compared the relative activation and recruitment of NF- κ B p65 (p65) to target genes by performing chromatin immunoprecipitation-sequencing (ChIP-seq) in ZIKV + and DENV + moDCs derived from two healthy donors. We detected significantly higher enrichment of p65 at 26,063 locations in DENV + moDCs compared with ZIKV + moDCs (4-fold enrichment and Poisson P -value < 0.0001), whereas only 399 sites in ZIKV + moDCs showed significantly greater p65 enrichment compared with DENV + moDCs (Fig. 3d). De novo motif analysis of the 26,063 sites demonstrated enrichment for motifs bound by NF- κ B p65 and AP-1 TFs (Supplementary Fig. 4a). To assess whether differences in p65 binding correlated with gene transcription, we compared p65 binding at genes that were expressed at higher levels in DENV + compared with ZIKV + moDCs ($n = 1031$), as well as genes expressed at similar levels in both virus + moDCs ($n = 11,279$) (Fig. 3a). Indeed, higher levels of p65 were bound near the transcription start sites of ~70% of the 1031 DENV-upregulated genes (Fig. 3e and f), whereas no differences in p65 binding were observed at the 11,279 genes similarly expressed in DENV + and ZIKV + moDCs (Supplementary Fig. 4b). The DENV-upregulated genes with increased p65 binding included cytokines such as *IL1B*, *IL12A*, and *IL6*; a chemokine receptor involved in DC migration, *CCR7*; and costimulatory receptors such as *CD40*, *CD80*, and *CD83* (Fig. 3g and Supplementary Fig. 4c).

We next determined whether ZIKV infection limited NF- κ B p65 activation and nuclear translocation. moDCs were infected with ZIKV or DENV for 24 h and analyzed by flow cytometry to confirm equivalent infection rates (4G2 + cells, Supplementary Fig. 4d). Live cells were sorted then fractionated into nuclear and cytoplasmic compartments and subjected to western blot analysis. Although NF- κ B p65 levels were similar in the cytoplasmic fractions of DENV- or ZIKV-infected cells ($n = 4$), p65 levels were significantly lower in the nuclear fraction of ZIKV-infected compared with DENV-infected moDCs (Fig. 3h–j). Thus, compared with DENV, ZIKV infection significantly impairs p65 nuclear localization as well as recruitment to and transcription of genes involved in DC activation and maturation.

We next investigated the ability of ZIKV to suppress NF- κ B p65 activation induced by the exogenous activators LPS and Kdo2-Lipid A (KLA), selective TLR4 agonists that activate NF- κ B signaling and induce DC maturation. First, expression of NF- κ B target genes in uninfected moDCs ($n = 4$ donors) incubated for 1 h with KLA was evaluated by RNA-seq, and this analysis identified 720 KLA-induced genes (2-fold upregulation and false discovery rate < 0.01). Comparison of these 720 genes with genes previously determined to be selectively upregulated

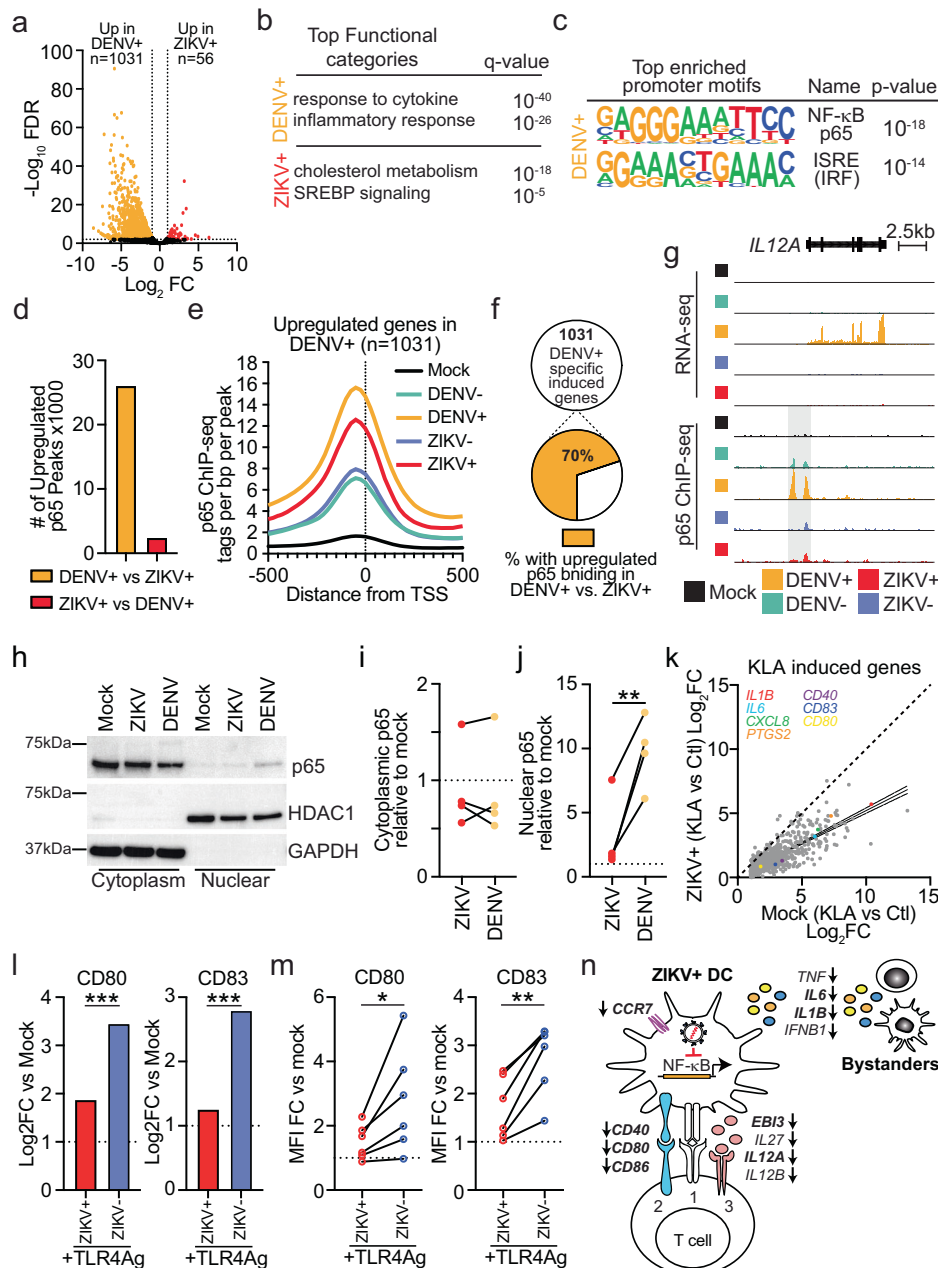


Fig. 3 | ZIKV Inhibits moDC Maturation and Function by Suppressing NF-κB p65 Nuclear Translocation and Function. **a** Volcano plot identifying differentially expressed genes in DENV+ compared with ZIKV+ moDCs at 24 h post-infection (hpi) as determined by RNA-seq. Data are expressed as the log₁₀ fold change (FC) relative to the false discovery rate (FDR) analyzed with DESeq2 ($n = 3$ donors). **b** Top two enriched pathways associated with DENV+ or ZIKV+ differentially regulated genes based on Metascape analysis. **c** Top enriched transcription factor motifs associated with DENV+ differentially upregulated genes determined by de novo motif analysis by HOMER using a one-sided binomial test. **d–g** NF-κB p65 ChIP-seq of moDCs infected with ZIKV PRVABC59 (MOI 0.5) or DENV2 UIS353 (MOI 1) for 24 h and sorted into DENV+, DENV-, ZIKV+, and ZIKV- populations ($n = 2$ donors). **d** Number of p65 binding sites with significantly increased reads in DENV+ vs ZIKV+ moDCs (4-fold enrichment and Poisson p -value < 0.0001). **e** Histogram of p65 binding relative to the annotated transcription start site (TSS) of genes upregulated in DENV+ compared with ZIKV+ moDCs (1031 genes significantly upregulated in DENV+ vs ZIKV+, fold change (FC) > 2 and FDR < 0.01). **f** Percentage of DENV-upregulated genes associated with upregulated p65 binding in DENV+ cells vs ZIKV+ moDCs. **g** UCSC browser visualization of the *IL12A* locus with RNA-seq and p65 ChIP-seq in mock, virus+, and virus- moDCs. Shaded areas represent the p65-binding regions. **h** Western blot analysis of NF-κB p65 subunit, HDAC1 (nuclear control), and GAPDH (cytoplasmic control) in subcellular fractions from control and

virus+ moDCs at 24 hpi. **i, j** Relative densitometric quantification of (i) cytoplasmic p65 and (j) nuclear p65 compared with mock cells at 24 hpi ($n = 4$). **k** Comparison of KLA-induced gene expression in mock-infected or ZIKV+ moDCs. KLA was added to cells for 1 h after mock, or ZIKV infection for 23 h. Log₂FC was determined by DESeq2 ($n = 4$ donors). A linear regression line with 95% confidence intervals is shown. **l** Relative mRNA expression (RNA-seq) of *CD80* and *CD83* in ZIKV+ and ZIKV- moDCs after KLA stimulation. KLA was added to cells for 1 h after ZIKV infection for 23 h. Data are expressed as the log₂FC relative to mock-infected cells with a two-sided false discovery rate (FDR) calculated by DESeq2 corrected for multiple hypothesis testing using the Benjamin-Hochberg correction. **m** Relative FC in mean fluorescence intensity (MFI) of *CD80* and *CD83* surface expression in ZIKV+ and ZIKV- moDCs infected for 24 h and then incubated with or without LPS for an additional 24 h. MFI FC is relative to mock-infected moDCs derived from the same donor. Circles represent the mean of duplicates from each donor ($n = 6$ donors). **n** Model for the effects of ZIKV-mediated NF-κB repression on moDC transcription of costimulatory molecules (signal 2), T cell-modulating cytokines (signal 3), proinflammatory cytokines, and DC migratory chemokine receptors. Down arrows denote decreased expression by RNA-seq, and bold indicates decreased p65 binding by ChIP-seq in ZIKV+ compared to DENV+ moDCs at 24 hpi. Source data and exact P -values are provided as a Source Data file.

in virus + moDCs showed that 9 (1.25%) of the KLA-induced genes were upregulated to a greater extent by ZIKV compared with DENV infection and 373 (51.8%) of the KLA-induced genes were upregulated to a greater extent by DENV compared with ZIKV infection (Supplementary Fig. 4e), which is consistent with our hypothesis that ZIKV infection results in suboptimal activation of NF- κ B in moDCs. To determine if ZIKV actively suppresses NF- κ B activation in infected cells, we stimulated uninfected or ZIKV-infected DCs with NF- κ B agonists and measured the upregulation of NF- κ B target genes. Comparison of gene expression in KLA-treated mock or ZIKV + moDCs (infection for 23 h and KLA treatment for 1 h) showed a striking suppression of KLA-induced genes, including the direct NF- κ B targets *IL6*, *IL1B*, *CXCL8*, *PTGS2*, *CD40*, *CD80*, and *CD83*, in ZIKV + moDCs compared with mock cells (Figs. 3k and l). Similarly, evaluation of LPS-stimulated mock or ZIKV + moDCs (infection for 24 h and LPS treatment for 24 h) showed that LPS-induced upregulation of CD80 and CD83 proteins was significantly lower in ZIKV + moDCs compared with mock cells (Fig. 3m). Taken together, these data indicate that, while NF- κ B p65 recruitment to and transcription of genes involved in inflammatory signaling and T cell antigen presentation is strongly induced by DENV infection, ZIKV infection suppresses p65 translocation to the nucleus and induction of p65-associated genes in moDCs (Fig. 3n).

ZIKV Infection of human moDCs limits their ability to stimulate allogeneic and antigen-specific T cell responses

The finding that ZIKV infection limits NF- κ B activation and expression of DC maturation- and function-associated genes suggested that the ability of moDCs to stimulate T cell responses might also be compromised by ZIKV infection. To test this hypothesis, we performed mixed leukocyte reactions (MLR) by co-culturing allogeneic human peripheral blood mononuclear cells (PBMC) with ZIKV + or DENV + moDCs (1:10 cell ratio) for either 1 or 3 days, and then examining the expression of T cell activation markers and secretion of cytokines by CD4⁺ and CD8⁺ T cells. PBMCs were stimulated with a combination of anti-CD3 and anti-CD28 antibodies as a positive control (Supplementary Fig. 5a). PBMCs incubated with ZIKV + moDCs for 1 or 3 days contained a significantly lower percentage of activated (CD69⁺) CD4⁺ and CD8⁺ T cells compared with MLRs containing DENV + moDCs (Figs. 4a and b and Supplementary Fig. 5a–c). Moreover, secretion of IFN γ on days 1 and 3 and of IL-2 on day 1 was significantly higher in MLRs containing DENV + compared with mock-infected moDCs, whereas no differences were observed in cytokine secretion by ZIKV + compared with mock moDCs (Fig. 4c and Supplementary Fig. 5d and 5e), indicating that ZIKV + moDCs had a reduced ability compared with DENV + moDCs to activate allogeneic T cells. To confirm these results, we co-stained for intracellular IFN γ or the cytolytic effector molecule granzyme B in activated (CD69⁺) CD4⁺ and CD8⁺ T cells. Indeed, the frequency of CD4⁺ IFN γ ⁺ (Fig. 4d and Supplementary Fig. 5f), CD8⁺ IFN γ ⁺ (Fig. 4e and Supplementary Fig. 5g), and CD8⁺ granzyme B⁺ (Fig. 4f and Supplementary Fig. 5h) T cells was markedly lower in MLRs containing ZIKV + moDCs compared with DENV + moDCs on days 1 and 3, although the differences in CD69⁺ CD8⁺ IFN γ ⁺ T cells on day 3 did not reach the level of statistical significance (Supplementary Fig. 5g).

To verify that the results obtained with allogeneic MLRs also extended to peptide-specific T cell responses, we examined the ability of virus + moDCs to stimulate antigen-specific responses by autologous T cells. To this end, ZIKV + or DENV + moDCs were cultured with megapools of diverse immunodominant class I and class II-restricted peptides, from organisms such as *Clostridium tetani*, Epstein-Barr virus, human cytomegalovirus, Influenza A, Coxsackievirus B4, *Haemophilus influenzae*, *Helicobacter pylori*, Human adenovirus 5, Human herpesviruses, Human papillomavirus, JC polyomavirus, Measles virus, Rubella virus, *Toxoplasma gondii* and Vaccinia virus (CEFT MHC II, CEF MHC I, EFX UltraSuper Stim, or SARS-

CoV-2 peptide pools; see “Methods”), then incubated with autologous T cells for 1 day, and then examined for T cell activation markers. Consistent with the MLR results, the percentage of activated (CD69⁺) CD4⁺ T cells (Fig. 5a–c) and CD8⁺ T cells (Fig. 5d–f) was higher after culture with DENV + moDCs compared with ZIKV + moDCs. Similarly, stimulation of IFN γ secretion was greater in the presence of peptide-cultured DENV + moDCs compared with ZIKV + moDCs (Fig. 5g and h). Taken together, these data demonstrate that ZIKV infection impairs the maturation and functional activation of moDCs and limits their ability to activate allogeneic and peptide-specific autologous T cells.

Discussion

In the present study, we compared the effects of ZIKV and DENV infection on the maturation and function of human DCs and macrophages, which are major host cells for flaviviruses and are crucial mediators of the host antiviral innate and adaptive immune responses. Recognition of microbial pathogens through intracellular and cell surface receptors triggers immature DCs to undergo a maturation program characterized by secretion of proinflammatory cytokines and upregulation of an array of cell surface molecules necessary for DC migration to the draining lymph nodes and subsequent activation of T cells⁴. We observed that ZIKV infection evoked much weaker transcriptional and functional responses in moDCs compared with those induced by DENV infection, and did so by suppressing NF- κ B nuclear translocation as well as recruitment to and transcription of a panel of crucial proinflammatory genes. Previous studies have evaluated the response of human DCs to infection with either DENV or ZIKV, but not both, and the results have been somewhat controversial. Specifically, some studies suggested that DENV blocked the activation of infected DCs and induced maturation only of uninfected bystander DCs^{3,11}, whereas other studies showed that DENV infection increased expression of HLA-DR and costimulatory factors by both infected and uninfected bystander DCs^{9,10,20}. Our results are consistent with two studies showing that ZIKV infection of human moDCs induced limited upregulation of cell surface MHC and costimulatory molecules^{7,8}; however, these studies did not address the mechanistic underpinnings or the impact on T cell activation. To address both the existing controversies and critical knowledge gaps, we undertook an unbiased genome-wide approach to identify changes in ZIKV + and DENV + moDCs compared with the corresponding uninfected bystander moDCs, and to evaluate both DENV and ZIKV infection of cells from multiple donors in parallel.

Our finding that ZIKV infection of moDCs induced a severely muted maturation program and functional DC response compared with DENV infection is consistent with our current understanding of ZIKV pathogenesis and, further, supports a key role for suppression of T cell responses in ZIKV pathogenesis. ZIKV-infected individuals exhibit only modest elevations of plasma IFN γ and various chemokines and no changes in TNF or IL-6 levels¹². A mouse study also demonstrated that a clinical ZIKV isolate (obtained from a Brazilian subject during the 2015 epidemic) actively suppresses CD8⁺ T cell responses by interfering with the maturation and antigen-presenting capacity of DCs, leading to delayed viral clearance¹⁴. This delay may enable ZIKV to establish sustained infection in its key target organs, namely, the maternal-fetal interface, brain, testis, and eye. The clinical relevance of our observations on ZIKV-mediated impairment of the human DC response is supported by studies of infected individuals in French Polynesia and Fiji, which revealed a significant decline in anti-ZIKV neutralizing antibody levels and herd immunity to ZIKV between 2015 and 2017¹³, whereas the same cohort maintained stable anti-DENV neutralizing antibody levels²¹. Because CD4⁺ T cells are necessary to promote a durable neutralizing antibody response as well as cytotoxic and memory CD8⁺ T cell responses against viruses²², our data provide evidence that the observed decline in anti-ZIKV neutralizing antibodies may result from suppression of DC-mediated activation of CD4⁺ T cells. In another smaller study, ZIKV-infected individuals ($n = 7$) had fewer

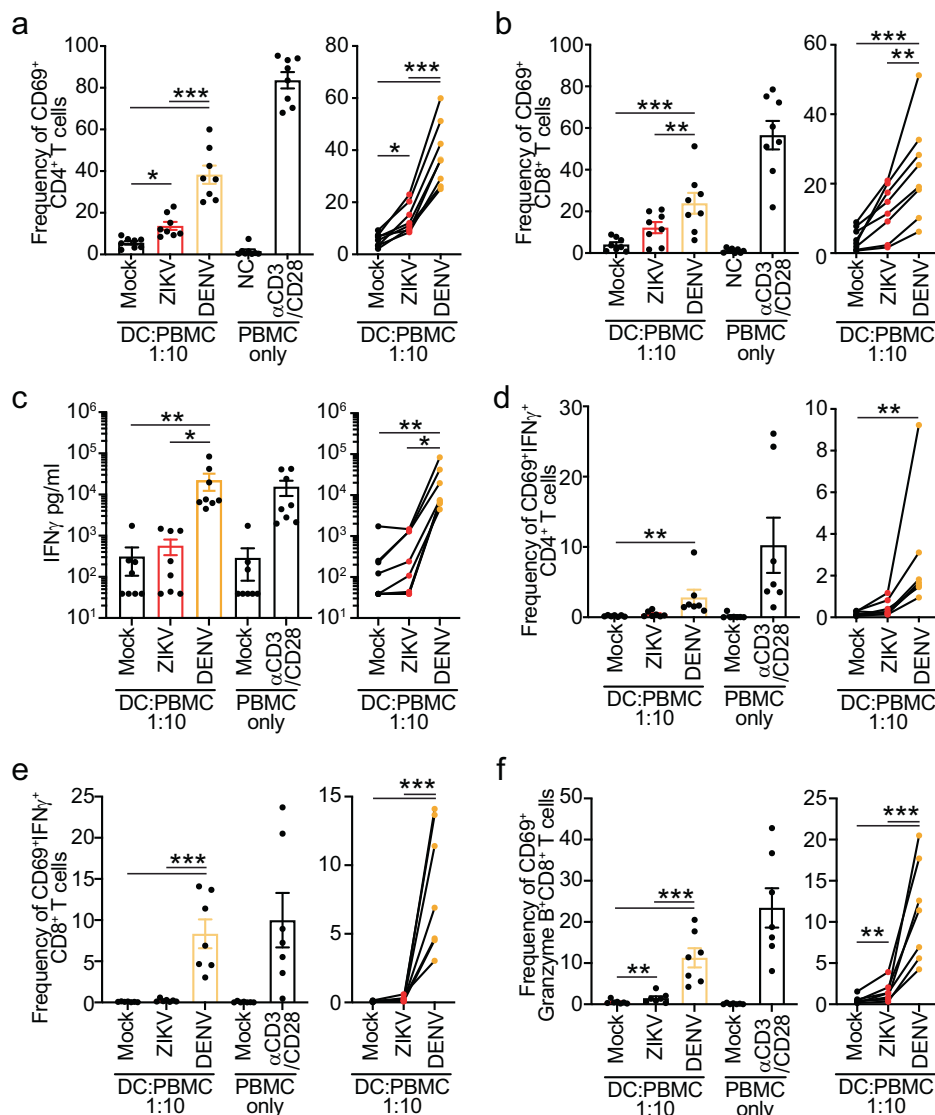


Fig. 4 | ZIKV Infection Severely Impairs the Ability of Human moDCs to Stimulate Proliferation, and Mediator Production by Allogeneic Peripheral T Cells. Mixed lymphocyte reactions were performed using immature moDCs mock-infected or infected with ZIKV SD001 or DENV2 UIS353 for 48 h plus freshly isolated allogeneic PBMCs at a ratio of 1 to 10 for 1 days. Unstimulated (NC) and anti (α)CD3/CD28-stimulated (α CD3/CD28) PBMCs served as negative and positive controls, respectively. Cells and culture supernatants were analyzed on days 1 and 3. **a, b** Frequency of activated (CD69⁺) (a) CD4⁺ T cells ($n = 8$ donors) or (b) CD8⁺ T cells ($n = 8$ donors) on day 1 of incubation determined by flow cytometry. **c** ELISA analysis of IFN γ concentrations in culture supernatants collected on day 1 of culture ($n = 8$ donors). **d–f** Flow cytometric analysis and quantification of (d)

activated CD69⁺ CD4⁺ T cells producing IFN γ ($n = 7$ donors) or (e) CD69⁺ CD8⁺ T cells producing IFN γ ($n = 7$ donors) or (f) granzyme B ($n = 7$ donors) on day 1 of culture. Data are presented as the mean \pm SEM, and circles represent the average of duplicates from each donor ($n = 6–8$ donors). Data from mock-, ZIKV-, and DENV-infected samples were compared using repeated measures one-way ANOVA with Tukey's correction for multiple comparisons (a, b, and e) or a Friedman test with Dunn's correction for multiple comparisons (c and d). Log-transformed mock-, ZIKV-, and DENV-infected samples were compared using repeated measures one-way ANOVA with Tukey's correction for multiple comparisons (f). * $P < 0.05$, ** $P < 0.01$, *** $P < 0.001$. Source data and exact P -values are provided as a Source Data file.

IFN γ -producing CD4⁺ T cells compared with DENV-infected individuals ($n = 5$)²³. Additional studies performed in mice support important roles for CD4⁺ and CD8⁺ T cell responses in protecting against ZIKV infection², including a requirement for both CD4⁺ T cells and IFN γ in the generation of anti-ZIKV neutralizing antibodies^{24,25}, and also support a role for a dampened CD4⁺ T cell response in the rapid waning of the anti-ZIKV neutralizing antibody response in humans. Thus, our data provide one possible explanation for the relative decline in anti-ZIKV compared with anti-DENV T cell and antibody responses documented in field studies^{13,23}.

Our finding that DENV infection of moDCs induced robust maturation and function is also consistent with our current understanding of DENV pathogenesis. The major pathophysiologic feature

of severe dengue is plasma leakage, although the precise mechanisms underlying endothelial cell dysfunction during the DENV inflammatory response are poorly understood. In DENV-infected individuals, elevated serum levels of TNF, IL-6, nitric oxide, and C-reactive protein have been reported to correlate positively with the severity of disease^{26,27}. Notably, increased levels of TNF, which mediates its effects via NF- κ B²⁸, were more frequent, and soluble TNF receptor levels were higher in plasma samples from patients with severe dengue than those with mild dengue or non-dengue febrile illnesses²⁹. In addition, neutralization of TNF was shown to prevent severe dengue-like lethal disease in mouse models of DENV infection^{30–33}. In the present study, we observed that DENV infection of human moDCs resulted in elevated production of proinflammatory mediators, including TNF.

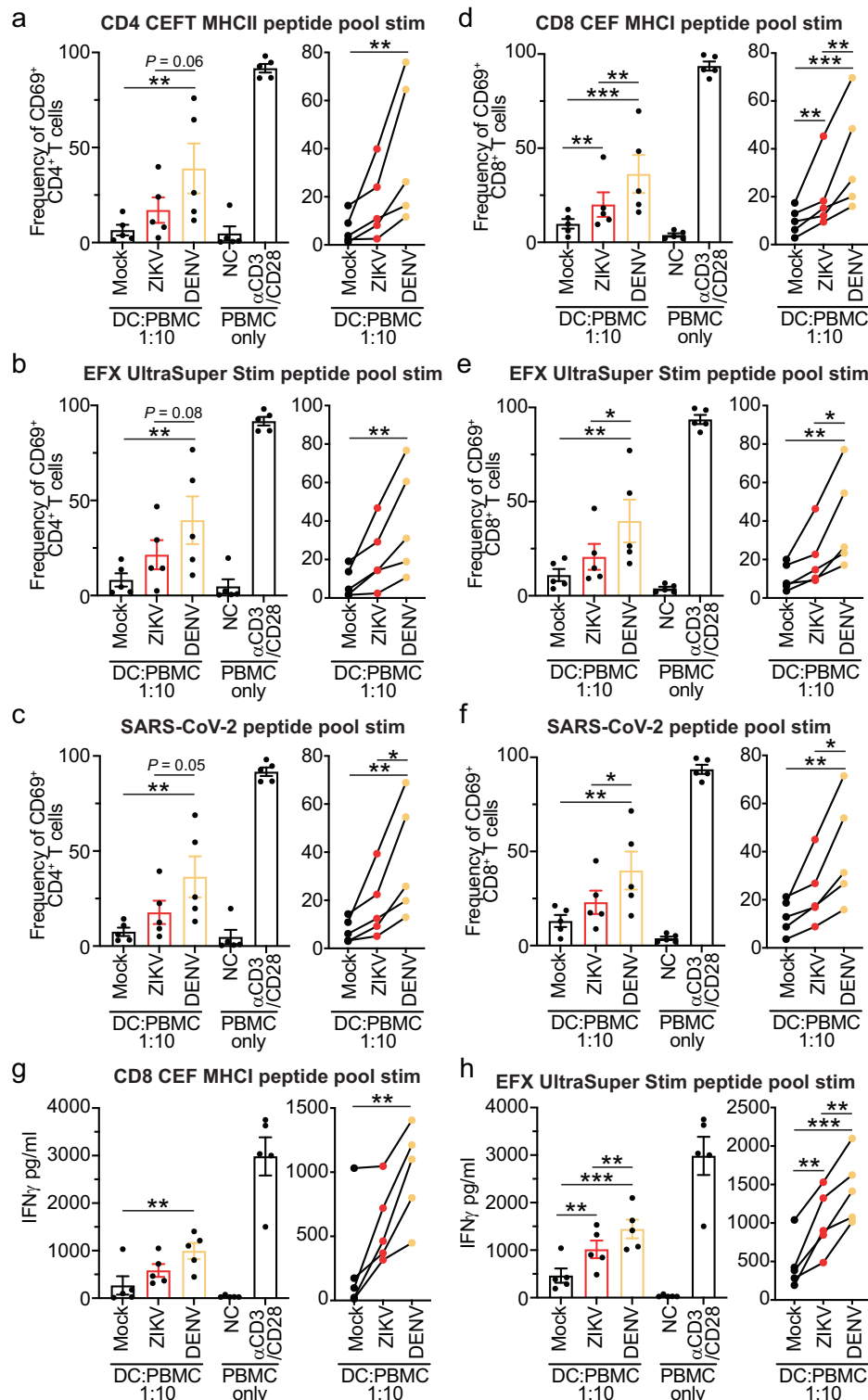


Fig. 5 | ZIKV Infection Inhibits the Ability of Human moDCs to Stimulate Autologous T Cell Responses. moDCs were infected with ZIKV SD001 (MOI of 0.5) or DENV2 UIS353 (MOI of 1) for 48 h and co-cultured with 10^6 autologous T cells and 10^5 moDCs in the presence of 1 μ g/ml of the indicated immunodominant peptide megapools. Unstimulated (peptide vehicle, DMSO) and anti (α)CD3/CD28-stimulated PBMCs served as negative and positive controls, respectively. After 24 h incubation, the frequency of activated (CD69⁺) CD4⁺ T cells (a–c) and CD8⁺ T cells (d–f) was determined by flow cytometry, and IFN γ concentrations in culture supernatants were determined by ELISA (g and h). Data are presented as the

mean \pm SEM, and circles represent the average of duplicates from each donor ($n = 5$). Data from mock-, ZIKV-, and DENV-infected samples were compared using repeated measures one-way ANOVA with Tukey's correction for multiple comparisons (a–c, e, f, and h) or a Friedman test with Dunn's correction for multiple comparisons (g). Log-transformed mock-, ZIKV-, and DENV-infected samples were compared using repeated measures one-way ANOVA with Tukey's correction for multiple comparisons (d). * $P < 0.05$, ** $P < 0.01$, *** $P < 0.001$. Source data and exact P -values are provided as a Source Data file.

Furthermore, by separating DENV+ and DENV- cells, our results show that DENV infection activates NF- κ B binding and transcription of target genes, such as *TNF* and *IL6*, primarily in DENV+ moDCs and macrophages. Consequently, higher levels of DENV infection in innate immune cells may be an important driver of systemic inflammation during severe DENV disease. Collectively, our data are consistent with clinical findings on DC-related functions in DENV-infected patients and suggest a link between innate immune cell dysfunction and severe dengue disease manifestations.

NF- κ B signaling regulates numerous critical cellular responses, including differentiation and death, and it is the key TF related to innate and adaptive immune responses to microbial pathogens^{34,35}. Accordingly, many viruses have evolved immune evasion strategies that modulate NF- κ B signaling³⁶. For example, infection with human immunodeficiency virus, hepatitis B and C viruses, influenza viruses, and respiratory syncytial viruses inhibits the NF- κ B pathway, preventing virus-induced host cell apoptosis and promoting virus replication³⁶. Conversely, DENV-induced activation of NF- κ B appears to be associated with the pathogenesis of severe dengue; specifically, DENV protease NS3 activates NF- κ B by inducing I κ B α and I κ B β cleavage and contributes to endothelial cell death³⁷. In the present study, we also observed strong p65 recruitment and NF- κ B activation in human moDCs following DENV infection, whereas ZIKV infection actively suppressed NF- κ B nuclear translocation and activation. ZIKV nonstructural proteins NS2A and NS4A (expressed via transient transfection) have been shown to downregulate NF- κ B promoter activation in HEK293T cells³⁸, suggesting that these two ZIKV proteins are the likely candidates responsible for inhibiting NF- κ B activation in the context of ZIKV infection of its natural host cells. Our results thus provide a foundation for identifying the precise ZIKV proteins and upstream components of the NF- κ B signaling pathway involved in suppressing the human DC response (e.g., recruitment of the adapters TRADD, RIP, and TRAF2, TRAF2-mediated recruitment of the IKK complex, and/or phosphorylation and degradation of I κ B α). Future studies should also determine whether ZIKV infection activates or suppresses the NF- κ B pathway in a host cell-dependent manner. In this regard, ZIKV infection of *Drosophila* results in an NF- κ B-dependent inflammatory response in the brain that restricts ZIKV replication by inducing STING expression³⁹, suggesting the possibility that NF- κ B signaling in ZIKV-infected human neuronal cells may also be induced rather than inhibited. Thus, NF- κ B activation or suppression may differ depending on the cell type (e.g., neuron *vs* DC) and species (e.g., fruit fly *vs* human; invertebrate *vs* vertebrate). Future studies using *Aedes* mosquitoes and a variety of relevant human cellular hosts should determine the precise role of NF- κ B in DENV and ZIKV pathogenesis.

In conclusion, our study provides insights into the strikingly different effects of two related and co-circulating flaviviruses on human DCs. Studies examining divergent effects of flaviviruses on NF- κ B-mediated pathways in distinct host cells will be of vital importance for deciphering the pathogenic mechanisms underlying flavivirus-induced diseases manifestations and for developing therapies and infection prevention strategies, particularly pan-flavivirus vaccines.

Methods

Isolation of primary human monocytes and differentiation of moDCs and macrophages

Human blood was collected from healthy donors (negative for human immunodeficiency virus, hepatitis B, and hepatitis C) under Protocol VD-057-0217 from the La Jolla Institute for Immunology and Protocol 181624 from UC San Diego. All recruited volunteers provided written informed consent. PBMCs were isolated by density gradient centrifugation on Histopaque 1077, and monocytes were purified by negative selection using a Human Pan Monocyte Isolation kit [Miltenyi Biotec, cat. #130-096-537] according to the manufacturer's instructions.

For moDC differentiation, monocytes were resuspended in complete RPMI medium [RPMI 1640 with GlutaMAX [Thermo Fisher Scientific, cat. #61870036], 10% (v/v) fetal bovine serum [FBS; Gemini Bioproducts, cat. #A82G00K], 2.5% (v/v) HEPES buffer [Gibco, cat. #15630-080], and 1% (v/v) penicillin/streptomycin [Gibco, cat. #15140-122] supplemented with recombinant human granulocyte-macrophage colony-stimulating factor (rhGM-CSF) 100 ng/ml [Pepro Tech, cat. #300-03] and recombinant human IL-4 (rhIL-4) 100 ng/ml [Pepro Tech, cat. #200-04], plated at 1.5×10^6 cells/ml in 6-well plates and incubated at 37 °C in a 5% CO₂ atmosphere for 7 days. The medium was changed after 3–4 days. Differentiation of CD14⁺ CD1a^{high} immature moDCs was confirmed on day 7 of culture by flow cytometry, as described below.

For macrophage differentiation, monocytes were resuspended in a complete macrophage medium (RPMI 1640 with L-glutamine [Corning, cat. #10-040-CV], 1% (v/v) penicillin/streptomycin [Gibco, cat. #15140-122], non-essential amino acids [Gibco, cat. #11140-050], and 10% (v/v) FBS [Biowest, cat. #S1620] supplemented with 100 ng/ml freshly-added recombinant human macrophage colony-stimulating factor (rhM-CSF) [PeproTech, cat. #300-25]. Cells were plated at 8×10^4 cells/well, 4×10^5 cells/well, or 8×10^5 cells/well in 96-, 24-, or 12-well plates, respectively, and allowed to differentiate for 7 days at 37 °C in a 5% CO₂ atmosphere. Medium was replaced every 3–4 days.

Virus propagation and focus-forming assay

ZIKV SD001 is an Asian lineage strain isolated in 2016 from a visitor to Venezuela returning to California, USA⁴⁰; ZIKV FSS13025 is an Asian lineage strain isolated from a patient in Cambodia in 2010 and was obtained from the World Reference Center for Emerging Viruses and Arboviruses; ZIKV PRVABC59 is an Asian lineage strain isolated from a patient in Puerto Rico in December 2015 and was obtained from BEI Resources. The African lineage ZIKV Dakar-1984 (Senegal, 1984) and DENV2 UIS353 (Colombia, 2004) strains were obtained from the World Reference Center for Emerging Viruses and Arboviruses. All viruses were propagated in C6/36 *Aedes albopictus* mosquito cells using standard conditions⁴¹.

Viral titers were measured using a baby hamster kidney (BHK)-21 cell-based focus-forming assay as previously described⁴¹. Briefly, BHK-21 cells were resuspended in complete MEM α [Thermo Fisher Scientific, cat. #12-561-072] containing 10% (v/v) FBS, 1% (v/v) HEPES buffer, and 1% (v/v) penicillin/streptomycin, plated at 2×10^5 cells/400 μ l/well in 24-well plates, and incubated overnight at 37 °C. Ten-fold serially diluted culture supernatants or viral samples were added to the cells and the plates were incubated with shaking every 15 min for 1 h at 37 °C. The supernatants were removed, and the cells were overlaid with 1 ml/well of 1% (w/v) carboxymethyl cellulose (Sigma, cat. #C5678) in a medium and incubated at 37 °C for 3 days. The cells were then fixed with 4% formalin, permeabilized with 1% Triton X-100, blocked with PBS/10% FBS, and incubated with clone 4G2 anti-pan-flaviviral envelope (E) protein [Absolute Antibody, cat. #Ab00230] at 1 μ g/ml for 1 h at room temperature. The cells were washed and incubated with horseradish peroxidase (HRP)-conjugated goat anti-mouse IgG secondary antibody [Jackson ImmunoResearch, cat. #115-035-072] at room temperature for 2 h. The cells were then stained with KPL True Blue peroxidase substrate [SeraCare Life Science, cat. #5510-0050] and foci were counted manually. Viral titers were expressed as focus-forming units per ml of sample.

Cell infection and flow cytometry of moDCs and macrophages

On day 7 of culture, moDCs were infected with ZIKV SD001, ZIKV FSS13025, ZIKV Dakar-1984, or ZIKV PRVABC59 (all at MOI of 0.5), or with DENV2 UIS353 (MOI of 1) for 2 h at 37 °C, washed once, and resuspended in complete RPMI medium. The cells were then placed in 24-well plates at a density of 5×10^5 cells/0.5 ml/well and incubated at

37 °C for the indicated times. Uninfected moDCs treated with vehicle (medium) or LPS [InvivoGen, cat. #tlrl-eb1ps] at 1 µg/ml served as controls. At 24 or 48 hpi, culture supernatants were collected and stored at –80 °C for analysis. MoDCs were collected, washed once with PBS, and stained with eFluor 455UV viability dye [Invitrogen, cat. #65-0868-14]. The cells were surface-stained with combinations of anti-CD80-PE [clone 2D10, BioLegend], anti-CD86-PerCP-Cy5.5 [clone IT2.2, BioLegend], anti-CD40-APC-Cy7 [clone 5C3, BioLegend], anti-CD83-BV421 [clone HB15e, BioLegend], and anti-HLA-DR-PE/Cy7 [clone G46-6, BD Bioscience]. The cells were then fixed and permeabilized using Cytofix/Cytoperm [BD Bioscience, cat. #554714] and intracellularly stained with AF647-conjugated 4G2 at 5 µg/ml for 20 min at 4 °C. All antibodies were prepared in 200-fold dilution. Data were acquired on an LSRFortessa and analyzed using FlowJo software v10.3. Where indicated, IL-6 [BD Bioscience, cat. #555220] and TNF [BD Bioscience, cat. #555212] in the culture, supernatants were quantified using cytokine-specific ELISAs according to the manufacturer's instructions.

On day 7 of culture, differentiated macrophages were infected with ZIKV SD001 or DENV2 UIS353 at a MOI of 1 (both viruses) via ADE. Viruses were mixed with predetermined optimal concentrations of anti-flavivirus E protein antibody, 5 µg/ml for ZIKV or 0.156 µg/ml for DENV [human IgG1-4G2, Absolute Antibody, cat. # Ab00230-10.0], in complete macrophage medium (as above except 1% FBS) and incubated at 37 °C, 5% CO₂ for 1 h. The medium was then removed from macrophages in 96-, 24-, or 12-well plates, and the virus/antibody mixture was added at 40, 250, or 500 µl/well, respectively. Control macrophages received mock infection, consisting of Conditioned medium ("mock" viral preparation; medium incubated 7 days on uninfected C6/36 cells and concentrated by the identical PEG purification procedure used for preparation of concentrated DENV and ZIKV stocks) incubated without antibodies in macrophage medium in place of virus/antibody mixture. The plates were incubated with rocking at 37 °C for 1 h, the virus/antibody supernatant was removed, and the macrophages were washed once in PBS before the addition of fresh complete macrophage medium. For intracellular cytokine staining, the cells were incubated for 18 h in medium alone and then for an additional 6 h in the presence of 3.0 µg/ml brefeldin A [ThermoFisher, cat. #00-4506-51]. At 24 hpi, macrophages were collected by scraping, stained with Zombie Violet Fixable Viability dye [BioLegend, cat. #423113], incubated with Human TruStain FcX Fc Receptor Blocking Solution [BioLegend, cat. #422302], and surface-stained with anti-CD80-PE [ThermoFisher Scientific, cat. #12-0809-42]. The cells were then fixed with Cytofix [BD, cat. #554655], permeabilized with BD PermWash [cat. #554723], and stained intracellularly with 1 µg/ml 4G2-AF647 (as above) plus either 1.25 µg/ml anti-IL-6-FITC [BioLegend, cat. #501103] or 2.5 µg/ml anti-TNF-AF488 [BioLegend, cat. #502917]. Data were acquired on a Sony MA900 flow cytometer and analyzed using FlowJo software v10 (TreeStar).

qRT-PCR

At 24 hpi, total RNA was isolated from macrophages using a Direct-Zol RNA micro-prep kit [Zymo, cat. #R2062] and RNA was reverse transcribed using an iScript kit [Bio-Rad, cat. #1708891]. qPCR was performed on an Applied Biosystems QuantStudio 5 Real-time PCR system [ThermoFisher Scientific] using iTaq Universal SYBR Green Supermix [Bio-Rad cat. #1725121] with the following primers: ribosomal protein lateral stalk subunit PO (RPLP0) forward 5'-GTGTTCCGACAATGGCAG CAT-3'; RPLP0 reverse 5'-GACACCCTCCAGGGAGCGA-3'; CD80 forward 5'-ATCCTGGGCCATTACCTTAATC-3'; CD80 reverse 5'-CTCTCATTCCTC CTCTCTCTCT-3'; IL-6 forward 5'-AGACAGCCACTCACCTCTTCAG-3'; IL-6 reverse 5'-TTCTGCCAGTGCCTCTTTGCTG-3'; TNF forward 5'-CTCT TCTGCCTGCTGCACCTTG-3'; TNF reverse 5'-ATGGGCTACAGGCTTGTC ACTC-3'; and IL-1-beta forward 5'-CCACAGACCTTCCAGGAGAATG-3'; IL-1-beta reverse 5'-GTGCAGTTCAGTGATCGTACAGG-3'.

Western blot analysis

moDC were infected with ZIKV PRVABC59 or DENV-PL046 for 24 h and stained with Zombie Violet™ Fixable Viability stain [BioLegend, cat. #423113] or 7-AAD Viability Staining Solution [BioLegend, cat. #420403] for 20 min at 4 °C. Live cells were then sorted using a SONY SH800S Cell Sorter (≥10⁶ cells per condition) and subjected to sub-cellular fractionation using NE-PER Nuclear and Cytoplasmic Extraction Reagents [Thermo Scientific, cat. #78833] per the manufacturer's instructions. A sample of the moDCs was fixed, permeabilized, and stained with 4G2-AF647 antibody as described above to determine the infection rate. Nuclear and cytoplasmic cell fractions containing Complete protease inhibitor [Sigma, cat. # 0469316001] were heated for 10 min at 70 °C in LDS sample buffer [Invitrogen, cat. #0007] and proteins were then separated on Bolt 4–12% Bis-Tris Plus gels and transferred to PVDF membranes. The membranes were blocked in a blocking buffer composed of 1x Tris-buffered saline [Fisher cat. #BP2471-1] plus 0.1% Tween 20 plus 5% non-fat milk [Research Products International, cat. #M17200-500.0], for 1 h at room temperature and then incubated at 4 °C overnight with primary antibodies: histone deacetylase (HDAC1) control nuclear protein [Cell signaling Technology, cat. #5356], glyceraldehyde 3-phosphate dehydrogenase (GAPDH) control cytoplasmic protein [Cell Signaling Technology, cat. #5174], or NF-κB p65 [Cell Signaling Technology, cat. #8242] all at 1:1000 dilution in blocking buffer. The membranes were washed again and incubated with HRP- or fluorophore-conjugated anti-rabbit or anti-mouse secondary antibodies [IRDye 800CW Goat anti-Mouse IgG Secondary Antibody, LI-COR, cat. # NC0824545; IRDye 680RD Goat anti-Rabbit IgG Secondary Antibody LI-COR, cat. # NC0885458; Goat anti-Rabbit IgG (H + L) Secondary Antibody, DyLight 800, ThermoFisher, cat. # SA535571; Peroxidase AffiniPure goat anti-mouse IgG, F(ab)₂ fragment-specific, Jackson ImmunoResearch, cat. #115-035-072; Goat Ant-Rabbit, Polyclonal Immunoglobulins, HRP, Agilent, cat. #044801-2] at 1:10,000 for 1 h at room temperature. Protein detection was performed using a ChemiDoc MP Imaging System, and the data were analyzed with Image Lab 6.0.1 [both Bio-Rad].

Mixed leukocyte reaction

moDCs were infected with ZIKV SD001 (MOI of 0.5) or DENV2 UIS353 (MOI of 1) for 48 h and mixed with freshly prepared allogeneic PBMCs at a ratio of 1:10 (5 × 10⁴ moDCs, 5 × 10⁵ PBMCs) in 200 µl complete RPMI medium containing 10% human serum (Innovative Research) in 96-well round-bottom plates. PBMCs mixed with uninfected moDCs and anti-CD3/CD28 (1 µg/ml each)-stimulated PBMCs served as controls. After 1 or 3 days, MLR cultures were spun down, and culture supernatants were collected. IL-2 and IFN γ levels in the culture supernatants were quantified by ELISA (BD Bioscience). The cells were resuspended with fresh medium containing 5 µg/ml brefeldin A [BioLegend] for an additional 6 h at 37 °C and then stained with eFluor 455UV viability dye [Invitrogen, cat. #65-0868-18], anti-CD3 PerCP-Cy5.5 [clone HIT3a, BioLegend], anti-CD4 eF450 [clone OKT4, Thermo Fisher Scientific], anti-CD8 APC-Cy7 [clone HIT8a, BioLegend], anti-CD69 BV785 [clone FN50, BioLegend], followed by fixation and permeabilization with the Cytofix/Cytoperm kit [BD]. The cells were then stained intracellularly with a combination of anti-IFN γ PE or FITC [clone 4S.B3, BioLegend], anti-IL-2 BV711 [clone MQ1-17H12, BioLegend], and anti-granzyme B AF647 [clone QA16A02, BioLegend]. All antibodies were diluted 200-fold for staining. Data were acquired on an LSRFortessa and analyzed using FlowJo software.

Antigen-specific T cell stimulation

moDCs infected with ZIKV SD001 (MOI of 0.5) or DENV2 UIS353 (MOI of 1) for 48 h were prepared as described above. Autologous T cells were negatively selected [STEMCELL, cat. #19051] from fresh PBMCs (same individual as for moDC preparation) and co-cultured with the

infected moDCs with 1 µg/mL of defined immunodominant peptide megapools [CD4 peptide pool: JPT, cat. #PM-CEFT-MHCII-3, including 14 peptide sequences derived from *Clostridium tetani*, Epstein-Barr virus, human cytomegalovirus, and Influenza A; CD8 peptide pool: Miltenyi Biotec, cat. #130-098-426, including 32 peptide sequences derived from Epstein-Barr virus, human cytomegalovirus, and Influenza A; EFX Ultra SuperStim Pool: JPT, cat. #PM-EFX-2, including 146 peptides from *Clostridium tetani*, Coxsackievirus B4, *Haemophilus influenzae*, *Helicobacter pylori*, Human adenovirus 5, Human herpesvirus 1, Human herpesvirus 2, Human herpesvirus 3, Human herpesvirus 4, Human herpesvirus 6, Human papillomavirus, JC polyomavirus, Measles virus, Rubella virus, *Toxoplasma gondii*, and Vaccinia virus; or SARS-CoV-2 peptide pool: Miltenyi Biotec, cat. #130-129-712] at a ratio of 10⁶ autologous T cells to 10⁵ moDCs in 96-well round-bottomed plates. Unstimulated controls consisted of T cells cultured with an equal concentration of peptide vehicle (DMSO). After 24 h, cell culture supernatants were collected for IFNγ quantification by ELISA, and the cells were stained with efluor 455UV viability dye [Invitrogen, cat. #65-0868-18], anti-CD3 AF700 [clone OKT3, BioLegend, cat. #317340], anti-CD4 BV605 [clone RPA-T4, BD Biosciences, cat. #562658], anti-CD8 BV650 [clone RPA-T8, BioLegend, cat. #301042], and anti-CD69 PE [clone FN50, BD Biosciences, cat. #555531]. Antibodies were stained at 200-fold dilution. Data were acquired on an LSRFortessa and analyzed with FlowJo software.

Cell sorting for RNA-seq and ChIP-seq

moDCs were collected from control or virus-containing cultures at the indicated times, stained with Zombie Violet™ Fixable Viability stain [BioLegend, cat. #423113] for 20 min at 4 °C, and washed. For RNA-seq, the cells were fixed and permeabilized with 4% paraformaldehyde and 0.1% saponin in the presence of RNasin Plus ribonuclease inhibitor (400 µl/ml; Promega, cat. #N2615), centrifuged, resuspended in wash buffer (0.2% BSA, 0.1% saponin, 400 µl/ml of RNasin Plus in PBS), and centrifuged. The supernatant was discarded, and the cells were resuspended in human Fc blocker buffer (1% BSA, 0.1% saponin, 1600 µl/ml RNasin Plus in PBS) for 5 min at 4 °C and incubated with 4G2-AF647 antibody for 30 min at 4 °C. The cells were centrifuged at 1000 × g for 3 min at 4 °C, resuspended in wash buffer, and re-centrifuged. Finally, the cells were resuspended in a sorting buffer (0.5% BSA and 1600 µl/ml RNasin Plus in PBS) and sorted into ZIKV+, DENV+, ZIKV-, or DENV- populations using a FACSAria [BD Biosciences]. For ChIP-seq experiments, washed moDCs were cross-linked with 4 mM disuccinimidyl glutarate in PBS for 30 min at room temperature, followed by 1% formaldehyde for 15 min at room temperature and quenched with 0.125 M glycine. The moDCs were then prepared and sorted into virus+ and virus- populations as described above for RNA-seq experiments, except the RNasin Plus inhibitor was replaced by 1x cComplete protease inhibitors [Roche, cat. #4693132001]. After sorting, the cells were washed in a sorting buffer, aliquoted into tubes at 5 × 10⁵ cells/sample, pelleted, snap-frozen, and stored at -80 °C.

NF-κB p65 ChIP-seq

Samples of 5 × 10⁵ cells were resuspended on ice in 500 µl RIPA buffer (50 mM Tris-HCl, pH 7.4, 1% IGEPAL CA-630, 0.25% sodium deoxycholate, 150 mM NaCl, 1 mM EDTA, 0.1% SDS, 0.5 mM DTT, 1x protease inhibitor cocktail). All subsequent steps were performed at 4 °C. Chromatin was sheared by sonication in epitubes using 14 cycles of 10 s at -13 W output and 30 s pause with a Sonic Dismembrator 60 [Fisher Scientific]. Samples were recovered and spun at 21,000 × g for 5 min, and the pellet was discarded. An aliquot of 2% of the sample volume was reserved as DNA input control and stored at -20 °C. To prepare antibody-coupled beads for ChIP, protein A Dynabeads [Invitrogen cat. #10002D], 20 µl per sample, were washed twice with 1 ml 0.5% BSA in TET (10 mM Tris-HCl, pH 8, 1 mM EDTA, 0.1% Tween 20), and resuspended in the same buffer. Anti-NFκB p65 antibody [C-20, Santa Cruz

Biotechnology cat. #sc-372] was added to the beads, and the sample was rotated for 1 h at room temperature. The supernatant was then removed, and the Dynabeads were collected using a magnet, washed once with 0.1% BSA/TET, and resuspended in 10 µl RIPA buffer. For ChIP, 10 µl of prepared antibody-conjugated Dynabeads was added to each sample and rotated overnight at 4 °C. The beads were then washed three times with 20 mM Tris-HCl, pH 7.4, 150 mM NaCl, 2 mM EDTA, 0.1% SDS, 1% Triton X-100, three times with 10 mM Tris-HCl, pH 7.4, 250 mM LiCl, 1 mM EDTA, 1% Triton X-100, 0.7% sodium deoxycholate, and twice with TET/0.2% (as above except 0.2% Tween 20). Dynabeads were resuspended in 25 µl TT (10 mM Tris-HCl, pH 8, 0.05% Tween 20). Input samples were resuspended in 25 µl TT, and libraries were generated in parallel with ChIP samples. Library NEBNext End Prep and Adapter Ligation were performed using NEBNext Ultra II DNA Library Prep kit [New England Biolabs, cat. #E7645L] according to the manufacturer's instructions with barcoded adapters [NextFlex, Bio Scientific. Cat. #514123]. Libraries were incubated with proteinase K at 55 °C for 1 h and then at 65 °C overnight to reverse formaldehyde crosslinks. Libraries were PCR amplified for 14 cycles with NEBNext High Fidelity 2X PCR MasterMix [New England Biolabs, cat. #NEBM0541]. Libraries were size selected for 200–400 bp fragments by gel extraction from 10% TBE gels [Life Technologies] and were single-end sequenced on an Illumina NextSeq 500 (San Diego).

RNA Isolation and library preparation for RNA-seq

Total RNA was isolated from cell pellets using a RecoverAll Total Nucleic Acid Isolation Kit [Invitrogen, cat. #AM1975] starting at the protease digestion step. All steps were performed according to the manufacturer's recommendations, except that cells were incubated for 3 h at 50 °C in digestion buffer supplemented with RNasin Plus (100-fold dilution). Thereafter, the RNA was treated with in-column DNase and eluted per the kit manufacturer's instructions. RNA quality was determined using a BioAnalyzer system [Agilent] with the Eukaryote Total RNA Pico Chip. Samples with RNA integrity values > 8.0 were used for library preparation. RNA libraries were generated using the TruSeq Stranded Total RNA Library Prep Kit (Illumina) kit, and single-end sequenced on an Illumina Hi-Seq 4000, NextSeq 500, or NovaSeq 6000, all according to the manufacturer's instructions.

NGS Data preprocessing

FASTQ files were mapped to the following reference genomes: UCSC build hg38 (human), GenBank KU955593.1 (ZIKV), or NC_001474.2 (DENV2). STAR with default parameters was used to map RNA-seq, and Bowtie2 with default parameters was used to map ChIP-seq data. HOMER was used to convert uniquely aligned reads into "tag directories" for further analysis.

Integrated NGS data analysis

RNA-seq reads aligned to a combined GRCh38/hg38 and either the ZIKV genome (KU955593.1) or DENV2 genome (NC_001474.2) were used to calculate the percentage of reads aligned to the ZIKV or DENV genome as follows: [(number of reads aligned to ZIKV or DENV genome / number of reads aligned to hg38 + ZIKV or hg38 + DENV genomes) × 100]. RNA-seq reads aligned to the GRCh38/hg38 assembly were used to generate gene expression FPKM values using HOMER⁴². To measure gene expression, HOMER's analyzeRepeats.pl utility was used to quantify reads in transcript exons defined by GENCODE. Differentially expressed genes and regularized logarithm (rlog) normalization values for each gene were calculated using DESeq2 while accounting for individual donors in the design matrix. NF-κB p65 ChIP-seq peaks were called from two biologic replicates of DENV- or ZIKV-infected samples with mock-infected conditions as the background (-b) and input DNA as input (-i) using HOMER's *getDifferentialPeaksReplicates.pl* with the "-style factor" and default parameters. Differentially regulated peaks between conditions were calculated by

first merging features from each condition (or assay) into the union of nonredundant features using *mergePeaks*. Then, differentially enriched peaks were compared between conditions using HOMER's *getDifferentialPeaks*⁴³. Known motif enrichment and de novo motif discovery were performed using HOMER's *findMotifsGenome.pl* utility with default parameters. NF- κ B p65 peaks were analyzed from ~100 to +100 base pairs relative to the center of the peaks, reflecting the locations where TFs and collaborating TF motifs are located. Normalized histograms of ChIP-seq peaks were generated using HOMER's *annotatePeaks.pl* and reported relative to a total of 10^7 uniquely aligned reads per experiment. Functional enrichment calculations were performed on differentially expressed genes (RNA-seq) and NF- κ B p65 ChIP-seq peaks using Metascape⁴⁴. Fold change values were clustered using Cluster 3.0⁴⁵ and visualized using Java TreeView⁴⁶.

Statistical analysis

Data were analyzed for distribution using normality and lognormality tests (D'Agostino–Pearson or Shapiro–Wilk) and compared using either a paired parametric *t* test or repeated measures one-way analysis of variance (ANOVA) with multiple comparisons test (indicated in each figure legend) or a paired non-parametric, Mann–Whitney or Friedman's test with Dunn's multiple comparisons test. Geometric mean and geometric standard deviation (SD) are shown for data plotted on a \log_{10} scale, and mean and standard error of the mean (SEM) or SD are shown for data plotted on a linear scale. Exact P-values are indicated or are categorically defined as: throughout as follows: not significant ($P > 0.05$), $*P < 0.05$, $**P < 0.01$, and $***P < 0.001$. All data were analyzed, and graphs were generated using Prism software v10 (GraphPad).

Reporting summary

Further information on research design is available in the Nature Portfolio Reporting Summary linked to this article.

Data availability

The human RNA-seq and ChIP-seq datasets described in this manuscript are available as [GSE161783](#) and [GSE220842](#) in the National Center for Biotechnology Information Gene Expression Omnibus. All data are included in the Supplementary Information or available from the authors, as are unique reagents used in this Article. The raw numbers for charts and graphs are available in the Source Data file whenever possible. Source data are provided in this paper.

References

- Pierson, T. C. & Diamond, M. S. The continued threat of emerging flaviviruses. *Nat. Microbiol.* **5**, 796–812 (2020).
- Elong Ngono, A. & Shresta, S. Immune response to Dengue and Zika. *Annu. Rev. Immunol.* (2018).
- Hilligan, K. L. & Ronchese, F. Antigen presentation by dendritic cells and their instruction of CD4+ T helper cell responses. *Cell Mol. Immunol.* **17**, 587–599 (2020).
- Inaba, K., Young, J. W. & Steinman, R. M. Direct activation of CD8+ cytotoxic T lymphocytes by dendritic cells. *J. Exp. Med.* **166**, 182–194 (1987).
- Schmid, M. A., Diamond, M. S. & Harris, E. Dendritic cells in dengue virus infection: targets of virus replication and mediators of immunity. *Front. Immunol.* **5**, 647 (2014).
- Sun, X. et al. Transcriptional changes during naturally acquired Zika virus infection render dendritic cells highly conducive to viral replication. *Cell Rep.* **21**, 3471–3482 (2017).
- Vielle, N. J. et al. Silent infection of human dendritic cells by African and Asian strains of Zika virus. *Sci. Rep.* **8**, 5440 (2018).
- Bowen, J. R. et al. Zika virus antagonizes type I interferon responses during infection of human dendritic cells. *PLoS Pathog.* **13**, e1006164 (2017).
- Ho, L. J. et al. Infection of human dendritic cells by dengue virus causes cell maturation and cytokine production. *J. Immunol.* **166**, 1499–1506 (2001).
- Libraty, D. H., Pichyangkul, S., Ajariyakhajorn, C., Endy, T. P. & Ennis, F. A. Human dendritic cells are activated by dengue virus infection: enhancement by gamma interferon and implications for disease pathogenesis. *J. Virol.* **75**, 3501–3508 (2001).
- Palmer, D. R. et al. Differential effects of dengue virus on infected and bystander dendritic cells. *J. Virol.* **79**, 2432–2439 (2005).
- Barros, J. B. S. et al. Acute Zika virus infection in an endemic area shows modest proinflammatory systemic immunoreactivation and cytokine-symptom associations. *Front. Immunol.* **9**, 821 (2018).
- Henderson, A. D. et al. Zika seroprevalence declines and neutralizing antibodies wane in adults following outbreaks in French Polynesia and Fiji. *Elife* **9**, <https://doi.org/10.7554/elife.48460> (2020).
- Pardy, R. D., Valbon, S. F., Cordeiro, B., Krawczyk, C. M. & Richer, M. J. An epidemic Zika virus isolate suppresses antiviral immunity by disrupting antigen presentation pathways. *Nat. Commun.* **12**, 4051 (2021).
- Carlin, A. F. et al. Deconvolution of pro- and antiviral genomic responses in Zika virus-infected and bystander macrophages. *Proc. Natl. Acad. Sci. USA* **115**, E9172–E9181 (2018).
- Carlin, A. F. & Shresta, S. Genome-wide approaches to unravelling host-virus interactions in Dengue and Zika infections. *Curr. Opin. Virol.* **34**, 29–38 (2019).
- Branche, E. et al. SREBP2-dependent lipid gene transcription enhances the infection of human dendritic cells by Zika virus. *Nat. Commun.* **13**, 5341 (2022).
- Gack, M. U. & Diamond, M. S. Innate immune escape by Dengue and West Nile viruses. *Curr. Opin. Virol.* **20**, 119–128 (2016).
- Harada, K. et al. Lipopolysaccharide activates nuclear factor- κ B through toll-like receptors and related molecules in cultured biliary epithelial cells. *Lab Invest.* **83**, 1657–1667 (2003).
- Chase, A. J., Medina, F. A. & Munoz-Jordan, J. L. Impairment of CD4+ T cell polarization by dengue virus-infected dendritic cells. *J. Infect. Dis.* **203**, 1763–1774 (2011).
- Kucharski, A. J. et al. Using paired serology and surveillance data to quantify dengue transmission and control during a large outbreak in Fiji. *Elife* **7**, <https://doi.org/10.7554/elife.34848> (2018).
- Swain, S. L., McKinstry, K. K. & Strutt, T. M. Expanding roles for CD4(+) T cells in immunity to viruses. *Nat. Rev. Immunol.* **12**, 136–148 (2012).
- Cimini, E. et al. Human Zika infection induces a reduction of IFN- γ producing CD4 T-cells and a parallel expansion of effector Vdelta2 T-cells. *Sci. Rep.* **7**, 6313 (2017).
- Lucas, C. G. O. et al. Critical role of CD4(+) T cells and IFN γ signaling in antibody-mediated resistance to Zika virus infection. *Nat. Commun.* **9**, 3136 (2018).
- Elong Ngono, A. et al. CD4+ T cells promote humoral immunity and viral control during Zika virus infection. *PLoS Pathog.* **15**, e1007474 (2019).
- Levy, A. et al. Increment of interleukin 6, tumour necrosis factor alpha, nitric oxide, C-reactive protein and apoptosis in dengue. *Trans. R Soc. Trop. Med. Hyg.* **104**, 16–23 (2010).
- Imad, H. A. et al. Cytokine expression in dengue fever and dengue hemorrhagic fever patients with bleeding and severe hepatitis. *Am. J. Trop. Med. Hyg.* **102**, 943–950 (2020).
- Vallabhapurapu, S. & Karin, M. Regulation and function of NF- κ B transcription factors in the immune system. *Annu. Rev. Immunol.* **27**, 693–733 (2009).
- Green, S. et al. Early immune activation in acute dengue illness is related to development of plasma leakage and disease severity. *J. Infect. Dis.* **179**, 755–762 (1999).

30. Shrestha, S., Sharar, K. L., Prigozhin, D. M., Beatty, P. R. & Harris, E. Murine model for dengue virus-induced lethal disease with increased vascular permeability. *J. Virol.* **80**, 10208–10217 (2006).
31. Ng, J. K. et al. First experimental in vivo model of enhanced dengue disease severity through maternally acquired heterotypic dengue antibodies. *PLoS Pathog.* **10**, e1004031 (2014).
32. Zellweger, R. M., Prestwood, T. R. & Shrestha, S. Enhanced infection of liver sinusoidal endothelial cells in a mouse model of antibody-induced severe dengue disease. *Cell Host Microbe* **7**, 128–139 (2010).
33. Watanabe, S. et al. Dengue virus infection with highly neutralizing levels of cross-reactive antibodies causes acute Lethal small intestinal pathology without a high level of viremia in mice. *J. Virol.* **89**, 5847–5861 (2015).
34. Hinz, M. & Scheidereit, C. The I κ B kinase complex in NF- κ B regulation and beyond. *EMBO Rep.* **15**, 46–61 (2014).
35. Mitchell, J. P. & Carmody, R. J. NF- κ B and the Transcriptional control of inflammation. *Int. Rev. Cell Mol. Biol.* **335**, 41–84 (2018).
36. Rahman, M. M. & McFadden, G. Modulation of NF- κ B signalling by microbial pathogens. *Nat. Rev. Microbiol.* **9**, 291–306 (2011).
37. Lin, J. C. et al. Dengue viral protease interaction with NF- κ B inhibitor α /beta results in endothelial cell apoptosis and hemorrhage development. *J. Immunol.* **193**, 1258–1267 (2014).
38. Lee, J. Y., Nguyen, T. T. N. & Myoung, J. Zika virus-encoded NS2A and NS4A strongly downregulate NF- κ B promoter activity. *J. Microbiol. Biotechnol.* **30**, 1651–1658 (2020).
39. Liu, Y. et al. Inflammation-induced, STING-dependent autophagy restricts Zika virus infection in the drosophila brain. *Cell Host Microbe* **24**, 57–68 (2018).
40. Carlin, A. F. et al. A longitudinal systems immunologic investigation of acute Zika virus infection in an individual infected while traveling to Caracas, Venezuela. *PLoS Negl. Trop. Dis.* **12**, e0007053 (2018).
41. Elong Ngono, A. et al. Mapping and role of the CD8⁺ T cell response during primary Zika virus infection in mice. *Cell Host Microbe* **21**, 35–46 (2017).
42. Heinz, S. et al. Simple combinations of lineage-determining transcription factors prime cis-regulatory elements required for macrophage and B cell identities. *Mol. Cell* **38**, 576–589 (2010).
43. Love, M. I., Huber, W. & Anders, S. Moderated estimation of fold change and dispersion for RNA-seq data with DESeq2. *Genome Biol.* **15**, 550 (2014).
44. Tripathi, S. et al. Meta- and orthogonal integration of influenza “OMICs” data defines a role for UBR4 in virus budding. *Cell Host Microbe* **18**, 723–735 (2015).
45. de Hoon, M. J., Imoto, S., Nolan, J. & Miyano, S. Open source clustering software. *Bioinformatics* **20**, 1453–1454 (2004).
46. Saldanha, A. J. Java Treeview—extensible visualization of microarray data. *Bioinformatics* **20**, 3246–3248 (2004).

Acknowledgements

This work was supported by a Career Award for Medical Scientists from the Burroughs Wellcome Fund (to A.F.C.), a fellowship from the Ministry

of Science and Technology of Taiwan 108-2917-I-564-032 (to Y.T.W.), an American Association of Immunologists Career Reentry Fellowship (to FASB), and NIH grants K08 AI130381 (to A.F.C.) and R01 AI116813, R01 AI153500, and R01 AI163188 (to SS) and LJI and Kyowa Kirin, Inc. (KKNA-Kyowa Kirin North America).

Author contributions

Y.T.W., A.F.C., and S.S. conceived the project. Y.T.W., E.B., J.X., R.E.M., A.F.C., S.H., and S.S. designed the experiments. Y.T.W., E.B., R.E.M., K.M.V., J.V.C., J.X., A.F.G., A.E.C., F.A.S.B., H.-H.L., Q.H.L., R.P.S.A., and A.F.C. performed the experiments. Y.T.W., E.B., J.X., K.M.V., R.E.M., A.F.C., and C.B. performed the data analysis. Y.T.W., A.F.C., and S.S. wrote the manuscript, with S.H. and C.B. providing editorial comments.

Competing interests

The authors declare no competing interests.

Additional information

Supplementary information The online version contains supplementary material available at <https://doi.org/10.1038/s41467-025-57977-2>.

Correspondence and requests for materials should be addressed to Aaron F. Carlin or Sujana Shrestha.

Peer review information *Nature Communications* thanks the anonymous reviewer(s) for their contribution to the peer review of this work. A peer review file is available.

Reprints and permissions information is available at <http://www.nature.com/reprints>

Publisher's note Springer Nature remains neutral with regard to jurisdictional claims in published maps and institutional affiliations.

Open Access This article is licensed under a Creative Commons Attribution-NonCommercial-NoDerivatives 4.0 International License, which permits any non-commercial use, sharing, distribution and reproduction in any medium or format, as long as you give appropriate credit to the original author(s) and the source, provide a link to the Creative Commons licence, and indicate if you modified the licensed material. You do not have permission under this licence to share adapted material derived from this article or parts of it. The images or other third party material in this article are included in the article's Creative Commons licence, unless indicated otherwise in a credit line to the material. If material is not included in the article's Creative Commons licence and your intended use is not permitted by statutory regulation or exceeds the permitted use, you will need to obtain permission directly from the copyright holder. To view a copy of this licence, visit <http://creativecommons.org/licenses/by-nc-nd/4.0/>.

© The Author(s) 2025